THE ASTROPHYSICAL JOURNAL, 302:727–736, 1986 March 15

HALOS AROUND PLANETARY NEBULAE

DAVID C. JEWITT,[1,2] G. E. DANIELSON,[2,3] AND P. N. KUPFERMAN[4]

Received 1983 June 10; accepted 1985 September 12

ABSTRACT

We report preliminary results of a CCD survey designed to detect and investigate faint halos around planetary nebulae. A TI 800 × 800 pixel CCD was used to take deep exposures of 44 planetary nebulae. The exposures were obtained through an Hα filter at the Cassegrain focus of the Palomar 1.5 m telescope. Spatial resolutions of 1″ to 2″ were obtained across 400″ wide fields. The images, which are in many cases considerably deeper than any previously taken, reveal numerous planetary nebula halos. About $\frac{2}{3}$ of the studied nebulae possess extensive outer halos, here defined as any extended emission beyond the 10% isophote. Ionized sulphur electron density measurements show that in some nebulae, the mass in the halo is comparable to the mass contained in the primary H II region. We have used the data to place constraints on the mode of origin of the halos. It is likely that the halos originate either by dynamical separation of a single ejected shell of gas or by the ejection of two or more such shells from the central star. It is possible but less likely that the halos are caused by excitation of the preplanetary stellar wind and improbable that the halos represent reflection nebulae.

Subject headings: nebulae: planetary — nebulae: reflection

I. INTRODUCTION

The morphologies of planetary nebulae have been the subject of numerous observational and theoretical investigations (Curtis 1918; Duncan 1937; Wilson 1950; Osterbrock, Miller, and Weedman 1966; Mathews 1966; Khromov and Kohoutek 1968; Weedman 1968; Greig 1971; Wentzel 1976, to name but a few). Observationally, the problem is to deduce the three-dimensional structures of the nebulae from their projections in the plane of the sky. The solution of this problem is made easier by the fact that the nebulae are optically thin at most wavelengths of observation. To some extent, Doppler velocity measurements can be substituted for the line-of-sight dimension, but the inversion problem is still intractable in many instances. A majority of the nebulae appear as elliptical rings in the plane of the sky. These are frequently interpreted to be thin, ellipsoidal shells of gas. Other interpretations include toroidal shells with their cylindrical symmetry axes near the line of sight. Some nebulae appear as centrally condensed objects; still others seem to be completely amorphous. Theoretical investigations have been confined to the most simple, spherically symmetric models and have had some success in matching the observed nebular expansions (Mathews 1966; Hunter and Sofia 1971).

In a number of planetaries, faint material can be observed projected outside the body of the main H II nebulae. These objects are known as double shell or halo nebulae and have received considerable attention. Nebulae reported to show faint halos include NGC 2392, 3242, 6809, 6804, 6720, and 7662 (Minkowski and Osterbrock 1960; Kaler 1974; Millikan 1974). Kaler (1974) suggests that the double shell nebulae result from a double pulse planetary nebula ejection process. In the case of NGC 7027, Atherton *et al.* (1979) suggest that the halo is a reflection nebulosity. Mathews (1966) notes that the halos may result from shock or radiation acceleration of the outer layers of the expanding primary shells. Kwok, Purton, and Fitzgerald (1978) suppose that the halos may be the illuminated escaping winds of the progenitor red giants.

An understanding of the halo nebulae may be important in the determination of the masses of the nebulae, and of their radii and lifetimes. Furthermore, since planetary nebulae are important contributors of material to the interstellar medium, the nature and frequency of the occurrence of the halos may be of importance to the study of the mass balance of the interstellar medium. However, despite the potential importance of the halo nebulae, relatively few such objects have been identified to the present time, and their status as normal components of the planetary nebulae is in doubt.

The present survey was designed to investigate a random sample of planetary nebulae, in a sensitive and systematic way, in order to determine the true frequency of occurrence of halo structures. The majority of halos described in this work have been observed by earlier workers. It is hoped that by systematically observing a number of these objects some common properties, perhaps indicative of the mode of origin, might be discerned.

II. OBSERVATIONS

a) Instrumentation

The observations were taken with a Texas Instruments 800 × 800 pixel charge-coupled device (CCD) during 1982 June–July. This CCD detector was characterized by very low readout noise (~10 electrons per pixel), good linearity of response (~0.1%), high sensitivity (quantum efficiency ~0.6 at 0.65 μm wavelength) and large dynamic range (~5000). Dark current was effectively eliminated by cooling the chip to 150 K with liquid nitrogen. For the present observations the CCD was mounted inside the versatile camera PFUEI (Gunn and Westphal 1981). PFUEI permitted observations in two distinct modes. As a direct camera the instrument was used to obtain images through narrow bandpass interference filters. As a spec-

[1] Department of Earth, Atmospheric, and Planetary Sciences, Massachusetts Institute of Technology.
[2] Palomar Observatory, California Institute of Technology.
[3] Division of Geological and Planetary Sciences, California Institute of Technology.
[4] Jet Propulsion Laboratory, California Institute of Technology.

trograph PFUEI was used to obtain low spectral resolution slit spectra of selected regions of the nebulae.

Most of the observations were acquired with the PFUEI at the Cassegrain focus of the 1.5 m telescope at Palomar Observatory. The f/8.75 focal ratio of the telescope was reduced to f/3.75 by a system of lenses in the PFUEI: the resulting image scale was 0".55 per 15 μm pixel at 0.65 μm wavelength. The field size was 440" square. In addition, a smaller number of observations were taken at the prime focus of the Hale 5.1 m telescope. With the Wynne corrector lens and PFUEI in place, an effective focal ratio of f/1.4 was obtained. The corresponding image scale and field width were 0".42 per pixel and 340", respectively. At both telescopes the final spatial resolution was determined by the atmospheric seeing. A journal of observations is given in Table 1.

b) *Images*

Planetary nebulae were selected from the atlas of Perek and Kohoutek (1967) according to two criteria: (1) the position of each object was chosen to satisfy the conditions $16^h00^m < \alpha_{1950} < 24^h00^m$ and $-25°00' < \delta_{1950}$, where α_{1950}, δ_{1950} are the right ascension and declination of the nebula at epoch 1950, and (2) the longest dimension of the nebular image, L (arcsec), was chosen to be in the range $10 < L < 200$. The latter criterion was implemented to ensure that a reasonable number of resolution elements were present across each nebular image and to exclude those nebulae which were substantially larger than the field of view (in retrospect, some nebulae proved to extend beyond the field of view at very low surface brightness levels; the outer halo of 96+29°1 [NGC 6543] was not recorded for this reason). It is possible, though unlikely, that a few of the objects selected from the Perek and Kohoutek catalog are not true planetary nebulae.

Observations in the direct camera mode were all taken through an interference filter centered at 6560 Å and having a full width at half-maximum (FWHM) = 98 Å and a peak transmission of 58%. This filter passed the Hα 6563 Å emission line as well as the [N II] 6548, 6583 Å emission lines from the nebulae, together with some nebular continuum.

In the direct imaging mode, short exposures were used to find and center each object in the field of view. A guide star was then acquired in an adjustable field eyepiece and was locked into position. In a few cases guiding was rendered impossible by the absence of suitable guide stars. Exposures of 1200 s duration were taken on each nebula. Complementary short exposures of nebulae having very high surface brightness were taken to prevent saturation of the CCD. The images were photometrically calibrated by taking short exposures of the standard stars BD +17°4708 and BD +26°2606. Flat field frames were recorded each time the PFUEI was mechanically adjusted to permit the subsequent removal of pixel to pixel response variations from the data frames. Numerous zero exposure "erase" frames were also recorded to permit subtraction of the bias level from the CCD.

Observations of bright stars were taken to determine the instrumental scattering function. Planetary nebula-like rings were simulated by exposing on out-of-focus star images. The exposures were used to guard against the possibility that any of the observed planetary nebula halos could be the result of light scattering within the telescope or camera. The internal scattering was found to be small in all but the most strongly saturated test exposures.

Two bright nebulae with halos were imaged through a polarizing sheet to attempt to detect gross polarization of the radiation. The polarizer was rotated 90° between exposures, and separate flat fields were recorded for each polarizer orientation. The data were not absolutely calibrated—instead the field stars within each image were used to provide relative intensity calibration between the two polarization frames. It was assumed that the field stars did not exhibit gross intrinsic polarization.

c) *Low-Resolution Spectra*

Low-resolution spectra were taken of many of the imaged nebulae in order to estimate the nebular electron densities from the [S II] 6716, 6731 Å line ratio. The dispersing element was a 600 lines per millimeter grating blazed at 5700 Å. It gave a dispersion of 4.3 Å per pixel and a useful wavelength range from 4300 Å to 7100 Å. The spectral resolution was determined by the width of the entrance slit. A 1" wide slit was used: the resulting spectrum lines had FWHM = 1.5 pixel corresponding to 6.4 Å. This resolution was sufficient to allow clear separation of the 6716, 6731 Å lines of [S II]. The 240" long slit permitted the simultaneous recording of the spectra of widely

TABLE 1

JOURNAL OF OBSERVATIONS

UT Date, 1982	Telescope (m)	Seeing FWHM (")	Sky Conditions	Work[a]
June 19–20	1.5	2.0	Cloud to photometric	Hα
June 22–23	1.5	1.0 to 2.0	Photometric	Hα
June 23–24	1.5	1.0	High cirrus	Hα POL
June 24–25	1.5	2.0	Photometric to cirrus	Hα, Hα POL
June 28–29	5.1	1.0	Photometric to cirrus	Hα
July 18–19	1.5	1.5	Photometric	Hα
July 19–20	1.5	2.0	Photometric	Hα
July 20–21	1.5	1.0	Photometric to cloud	Hα
July 21–22	1.5	1.5	Cirrus	Sp
July 22–23	1.5	1.2	Cirrus	Sp
July 23–24	1.5	1.8	Cloud	Sp
July 24–25	1.5	1.0 to 1.5	Photometric	Hα
July 26–27	1.5	1.5	Photometric	Hα, Sp
July 27–28	1.5	1.0	Photometric	Hα, Sp

[a] Hα, direct imaging; Hα *POL*, direct imaging through polarizer; Sp, spectrography.

separated regions of each nebula, with seeing limited resolution along the length of the slit. In most cases the slit was long enough to project onto the adjacent sky, thereby providing an independent, simultaneous night sky spectrum.

The positioning of the spectrograph slit on each nebula was achieved by using PFUEI as a direct finder camera. PFUEI was then converted to a spectrograph, and a short exposure was taken to confirm the correct positioning of the slit (usually by noting the location and appearance of the central star of the planetary). The positioning was found to be accurate to better than 1″ in declination and to about 1″ in right ascension. The slit was oriented east to west for all the observations reported here. Rather long exposures (1200–3600 s) were obtained to attempt to achieve good signal strengths in the [S II] lines. Flat field and erase frames were recorded in the same manner as for the direct frames. No attempt was made to obtain absolute flux calibration for the spectra, such calibration being precluded by the very narrow slit and by atmospheric effects.

III. RESULTS

a) *Interference Filter Images*

Images of 44 nebulae in the light of H I + [N II] are presented in Figure 1 (Plates 22–26). The panels in the figure should be read from left to right, then from top to bottom. Each image is shown in two versions in order to provide a basis for the systematic intercomparison of the nebulae. The first image of each object is a "stretch" between the sky brightness and the brightest part of the nebula; i.e., it displays all of the data numbers in the image of the nebula. In the second image only the lowest 10% of the data numbers are displayed; those above have been set equal to white in the figure. We define any material which extends beyond the 10% isophote of a primary nebula by a distance large compared to a seeing disk as halo material. Though arbitrary, this definition is a practical one, since a CCD image of a point source shows only slight extension beyond the 10% isophote. The presentation in Figure 1 thus emphasizes the bright primary structures in the first image and the faint secondary halos in the second. In a few nebulae, very faint halos are not well seen in either stretch of Figure 1. These halos are more clearly evident in Figure 2 (Plate 27), where only the lowest 1% of the data numbers are displayed. In both figures, pixels which are saturated in the raw data appear black. Strongly saturated images appear elongated east-west due to a property of the detector. Each nebula is accompanied by a scale bar of 20″ length and by a designation from the Perek and Kohoutek catalog.

The nebulae shown in Figure 1 exhibit a wide range of morphologies. For example, centrally condensed, ring, bipolar, and irregular nebulae are all present in the sample (see, for example, 21−0°1, 40−0°1, 10+18°2, and 85+4°1, respectively). Such pronounced variations of appearance make the intercomparison of the nebulae very difficult. In addition, the nebulae exhibit great structural complexity which thwarts much quantitative analysis of the images. In this work we are mostly concerned with ascertaining the gross properties of the halos. Consequently, we elect to describe each nebula by a few readily measured parameters, even though these may not fully reflect the true complexities evident in the images. The basic parameters have been chosen as follows.

a, b the semimajor and semiminor axes of the best fit ellipse to the 10% isophote;

p, q the semimajor and semiminor axes of the best fit ellipse to the edge of the halo material, where a halo is observed;

ϕ the position angle of the major axis of the best fit ellipse to the 10% isophote.

From the above quantities, which serve to describe the shapes of the primary nebulae and their halos, several secondary quantities have been computed and are listed in Table 2. These are

e_p, e_h the ellipticities of the primary nebulae and halos;

R_h, R_p the ratio of the averaged semiaxes of the primary nebulae and halos.

The ellipticities have been defined through

$$e_p = [1 - (a/b)^2]^{1/2}; \quad e_h = [1 - (p/q)^2]^{1/2}$$

and the equivalent circular semiaxes through

$$R_p = (ab)^{1/2}; \quad R_h = (pq)^{1/2} .$$

Other quantities listed in Table 2 include column (1), object designation from Perek and Kohoutek (1967); column (2), alternative designations; columns (3), (4), α, δ: right ascension and declination (epoch 1950); columns (5), (6), I^{II}, b^{II}: galactic longitude and latitude; column (7), ϕ: position angle of the primary long axis; column (8), θ: angle between the long axis and the galactic equator; column (9), indication of whether a halo is (Y) or is not (N) present; Column (10), Δ: distance to the nebula where known (Acker 1979); column (11), morphological type of the primary nebula determined by inspection of the CCD images. R = ring; I = irregular; C = centrally condensed; B = bipolar (cf. Greig 1971).

Excellent examples of halos, shown in Figure 1, are found in the nebulae 2+5°1, 8+3°1, 36−1°1, 64+48°1, 69−2°1, 83+12°1, 85+4°1, 89+0°1, and 106−17°1. In some nebulae the halos are circularly symmetric (e.g., 69−2°1, 83+12°1, 106−17°1), whereas in others the halos have an irregular or filamentary appearance and do not exhibit circular symmetry (e.g., 2+5°1, 8+3°1, 85+4°1). At least two extreme interpretations of the more irregular halos are possible: either (a) the irregular appearance is due to a truly irregular distribution of matter in the halos or (b) the irregular appearance results from azimuthal variations in the radial Lyman limit optical depth in the primary nebulae. The former case would correspond to a "density bounded" nebula, the latter to a "radiation bounded" nebula. In the latter case a complete spherical shell halo would appear to be irregular as a result of the patchy shadowing of ionizing radiation by material in the primary shell. Plausible examples of shadowing are found in 41−2°1 and 88−1°1. In both nebulae the position angles of faint sections of the primary nebulae are coincident with the position angles of bright sections of the respective halos. Other possible examples may be found in 8+3°1, 36−1°1, 68−0°1, 103+0°1, and 114−4°1. Counterexamples may be found in 33−6°1, 64+48°1, and 106−17°1.

The frequency distribution of the ratio R_h/R_p is plotted in Figure 3. The range is $1.2 < R_h/R_p < 5$ and the mean is 2.1 ± 0.2 ($n = 25$). The mean ellipticities of the primary nebulae and the halos are $e_p = 0.57 \pm 0.04$ ($n = 40$) and $e_h = 0.54 \pm 0.05$ ($n = 28$), respectively. These means are identical within the uncertainties. Hence, statistically, the halos are the same shape but about twice the diameter of their respective primary nebulae. The ratio of the halo to primary nebula surface brightnesses I_h/I_p exhibits wide variations within the range $10^{-3} < I_h/I_p < 0.1$.

TABLE 2

PROPERTIES OF NEBULAE

Object (1)	Name (2)	α_{1950} (3)	δ_{1950} (4)	l^{II} (5)	b^{II} (6)	ψ (7)	v^{∞} (8)	Halo (9)	Δ (kpc) (10)	Type (11)	R_p (12)	R_h (13)	R_h/R_p (14)	R_p (pc) (15)	e_p (16)	e_H (17)
2+ 5°1	6369	17 26.3	-23°43'	2.44	+5.85	74	-72	Y	1.2	R	17	34	2.00	0.10	0.31	0.42
8+ 3°1	6445	17 46.3	-20 00	8.07	+3.90	-10	21	Y	1.35	R	18	106	5.89	0.12	0.65	0.40
9+14°1	6309	17 11.3	-12 51	9.66	+14.81	-20	13	Y	2.6	I,C	16	45	2.81	0.20	0.85	0.81
10+18°2	M2-9	17 02.9	-10 04	10.91	+18.06	0	33	N	2.75	B	13	—	—	0.17	0.98	—
17-10°1	A51	18 58.1	-18 17	17.61	-10.24	—	—	N	—	R	31	—	—	—	0.19	—
21- 0°1	M3-28	18 29.9	-10 08	21.82	-0.47	0	28	Y	2.3	C	4	14	3.50	0.04	0.71	0.92
24+ 5°1	M4-9	18 11.6	-05 00	24.22	+5.95	-10	18	N	1.3	R	21	—	—	0.13	0.55	—
25- 4°2	IC1295	18 51.6	-08 51	25.42	-4.63	65	-88	Y	—	R	45	65	1.44	—	0.52	0.62
26+ 1°1	V-V1-8	18 30.6	-05 00	26.44	+1.77	-30	-2	Y	1.0	I	—	> 240	—	—	—	—
29+ 0°1	A48	18 40.2	-03 16	29.09	+0.45	60	87	N	—	R	10	—	—	—	0.65	0.60
33- 6°1	6772	19 12.0	-02 47	33.17	-6.38	10	37	Y	1.25	R	37	54	1.46	0.22	0.17	0.80
34+11°1	6572	18 09.7	+06 50	34.62	+11.84	-5	22	N	0.67	C	7	—	—	0.02	0.75	—
35- 0°1	Ap2-1	18 55.6	+01 33	35.13	-0.75	-50	-23	Y	—	C	14	19	1.36	—	0.57	0.54
36- 1°1	Sh2-71	18 59.5	+02 05	36.06	-1.37	-10	17	Y	—	R	67	194	2.90	—	0.84	0.40
38-25°1	A70	20 28.9	-07 16	38.11	-25.47	-25	2	N	—	R	21	—	—	—	0.55	—
40- 0°1	A53	19 04.3	+06 19	40.37	-0.47	—	—	N	—	R	15	—	—	—	0.00	—
41- 2°1	6781	19 16.0	+06 27	41.84	-2.98	-15	13	Y	0.80	R	60	79	1.32	0.23	0.49	0.77
45+24°1	K1-14	17 40.4	+21 28	45.59	+24.33	-20	1	N	—	R	26	—	—	—	0.20	—
50+ 3°1	M1-67	19 09.3	+18 47	50.21	+3.31	30	58	N	0.65	IR	57	—	—	0.18	0.40	—
59-18°1	A72	20 47.7	+13 22	59.80	-18.74	-15	20	N	—	R?	111	—	—	—	0.86	—
63+13°1	6720	18 51.7	+32 58	63.17	+13.98	60	84	Y	0.57	R	39	74	1.90	0.11	0.65	0.61
64+15°1	M1-64	18 48.2	+35 11	64.98	+15.53	-40	-17	Y	2.5	R	9	15	1.67	0.11	0.55	0.00
64+48°1	6058	16 02.7	+40 49	64.67	+48.30	-25	-22	Y	2.6	R	10	15	1.50	0.13	0.52	0.62
65+ 0°1	6842	19 53.0	+29 09	65.91	+00.60	—	—	Y	1.27	R	13	29	2.23	0.08	0.70	0.43
66-28°1	7094	21 34.5	+12 34	66.79	-28.21	—	—	N	1.3	R	49	—	—	0.31	0.18	—
68-0°1	M1-75	20 02.8	+31 19	68.86	-0.05	-30	3	Y	2.8	R	8	21	2.63	0.11	0.82	0.94
68+ 1°2	He1-4	19 57.3	+31 47	68.63	+1.19	-30	2	Y	1.8	R	11	14	1.27	0.10	0.50	0.38
69- 2°1	6894	20 14.4	+30 25	69.48	-2.62	—	—	Y	1.41	R	20	31	1.55	0.14	0.57	0.31
83+12°1	6826	19 43.5	+50 24	83.56	+12.78	—	—	Y	1.02	C?	$\lesssim$ 13	69	$\gtrsim$ 5.3	—	—	0.00
85+ 4°1	A71	20 30.8	+47 11	85.01	+4.49	20	56	Y	—	I	106	> 220	> 2.08	—	0.67	—
88- 1°1	7048	21 12.4	+48 04	88.76	-1.68	15	59	Y	1.3	R?	35	54	1.54	0.22	0.64	0.48
89+ 0°1	7026	21 04.6	+47 39	89.00	+0.37	-5	37	Y	1.67	R?	—	20	—	—	—	0.83
93+ 5°2	7008	20 59.1	+54 21	93.42	+5.49	15	56	Y	—	I	40	60	1.50	—	0.60	0.73
95+ 7°1	A73	20 55.2	+57 15	95.27	+7.80	15	55	N	—	R	40	—	—	—	0.49	—
96+29°1	6543	17 58.6	+66 38	96.47	+29.95	20	20	Y	0.65	R	6	12	2.00	0.02	0.80	0.79
97+ 3°1	A77	21 30.6	+55 40	97.52	+3.18	80	-53	N	—	I	28	—	—	—	—	—
101+ 8°1	A75	21 25.2	+62 40	101.85	+8.74	—	—	Y	—	I	18	35	1.94	—	0.62	0.00
102- 2°1	A79	22 24.4	+54 34	102.98	-2.33	65	-57	N	—	IR	25	—	—	—	0.40	—
103+ 0°1	M2-51	22 14.3	+57 14	103.23	+0.68	-20	36	Y	1.6	R	16	38	2.38	0.12	0.89	0.72
106-17°1	7662	23 23.5	+42 16	106.56	-17.60	35	-75	Y	1.15	R	7	17	2.43	0.04	0.75	0.48
107+ 2°1	7354	22 38.5	+61 01	107.84	+2.31	—	—	Y	1.6	I?	10	21	2.10	0.08	0.59	0.44
114- 4°1	A82	23 43.4	+56 47	114.07	-4.68	40	-65	Y	—	B	42	53	1.26	—	0.27	0.72
120+ 9°1	40	00 10.3	+72 15	120.02	+9.87	20	-79	N	0.92	R?	25	—	—	0.11	0.81	—
326+42°1	1972	14 01.7	-17 01	326.75	+42.21	—	—	Y	2.0	R	24	26	1.08	0.23	0.36	0.39

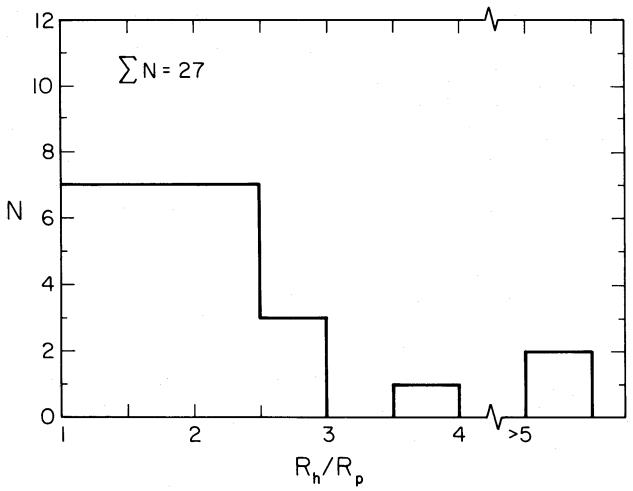

FIG. 3.—Distribution of the ratio of the halo radius R_h to the primary nebula radius R_p. The distribution is peaked toward small values of the ratio and has a mean equal to 2.

The distribution of the orientations of the apparent long axes of the nebulae is shown in Figure 4. The angle, θ, between the apparent long axis of each nebula and the galactic plane is also listed in Table 2. The dotted curve in Figure 4 represents the θ distribution to be expected if the nebular long axes are distributed randomly in direction. Evidently, the observed distribution is similar to the model curve, suggesting that there is no preferential alignment of the axes. This is opposite to the conclusion reached by Grinin and Zvereva (1968) and by Melnick and Harwit (1975), who found the long axes of planetary nebulae to be preferentially aligned in the galactic plane. Such an alignment would have provided (rather surprising) evidence for the control of nebular morphology by an external agency, possibly the interstellar magnetic field.

The variation of the nebular surface brightness as a function of radial distance from the central star has been investigated by examination of nearly circularly symmetric nebulae possessing halos. The surface brightness, $B(r)$, was averaged around concentric circles centered on each nebula center. Figure 5 contains plots of log $[B(r)]$ versus log (r) for six circular nebulae. The plots have been marked to show the location of the

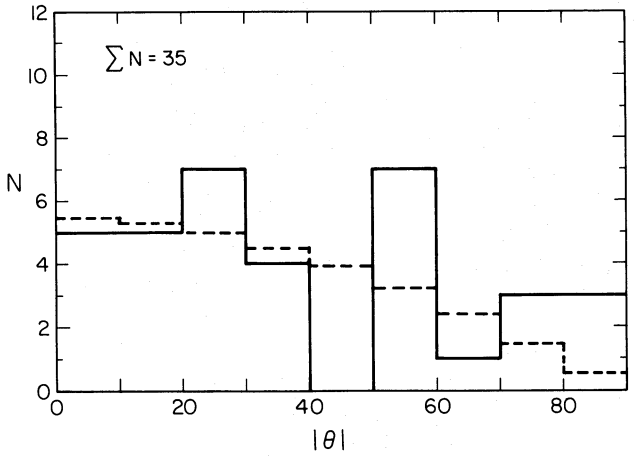

FIG. 4.—Distribution of the directions of the apparent long axes of the planetary nebulae. The number of nebulae, N, having their longest axes inclined to the galactic equator at angle θ is shown. The dashed line depicts the distribution to be expected if the longest axes are randomly oriented. Within the statistical uncertainties, the model and the observed distribution are similar.

boundary between the primary nebula and the halo in each instance. The plots show that the surface brightness of the halos decreases sharply with r, often more quickly than the inverse fifth power of r.

The majority of the halos are too irregular to allow the construction of meaningful plots of the type presented in Figure 5. Large variations of surface brightness occur over small distances in the halos. A common feature of many of the halos, shown in Figures 1 and 2, is the presence of loop filaments. The loop filaments appear convex outward, have radii equal to a fraction of R_p, have widths comparable to the seeing, and often appear to have centers of curvature close to the primary/halo boundaries. Examples may be seen in 2+5°1, 33−6°1, 68−0°1, 89+0°1, 103+0°1, and 120+9°1 (in Fig. 1) and in 8+3°1, 9+14°1, 63+13°1, and 83+12°1 (in Fig. 2). Many of the halo electron density measurements discussed in § IIIc refer to loop filaments rather than to the fainter surrounding material. The origin of the loops is unclear but their resemblance to shock fronts is striking.

b) *Polarizations*

Images of the nebulae 63+13°1 and 64+48°1 taken through perpendicular polarizers were scaled by equalizing the intensities of field stars (assumed to have negligible polarization). Scale factors determined from different field stars were equal to within 1%. The scaled frames were then subtracted. Residual differences in the subtracted images were attributable to registration errors. They place an approximate upper limit to the degree of linear polarization present in the nebular Hα + [N II] radiation of $POL < 0.05$. This upper limit is consistent with the typical primary nebula polarization of about 1% (Hamilton and Liller 1972). The significance of the absence of larger polarization in the halos of these nebulae will be discussed in § IV.

c) *Optical Spectra*

The optical spectra were examined with the principal objective of measuring the halo electron densities. This was achieved by determination of the ratio of the intensities of the [S II] 6716, 6731 Å lines. In the majority of the spectra, these lines were sufficiently faint that small-scale variations along the spectrograph slit could not be separated from the pixel to pixel noise. In these spectra, the ratio of the line intensities was obtained by the averaging of long segments (typically ≈ 10″) of the slit images.

The unresolved electron measurements are presented in Table 3. The contents of the table are column (1), object designation (Perek and Kohoutek 1967); column (2), Δα (arcsec): the offset of the center of the spectrograph slit from the central star, in right ascension; column (3), Δδ (arcsec): the offset of the center of the spectrograph slit from the central star, in declination; column (4), L (arcsec): the length of the slit along which the [S II] line intensities were averaged. The slit was always aligned east-west on the sky and was of 1″ width; column (5), r/R_p: where $r = (\Delta\alpha^2 + \Delta\delta^2)^{1/2}$ is the separation between the central star and the effective center of the slit. R_p is the radius of the primary nebula in arcsec (from Table 2); column (6), the type of material sampled by the spectrograph slit, either primary nebula (P) or halo (H); column (7), [S II] (6717/6731): the ratio of the intensities of the [S II] lines within the effective slit. The tabulated uncertainties were computed by assuming a

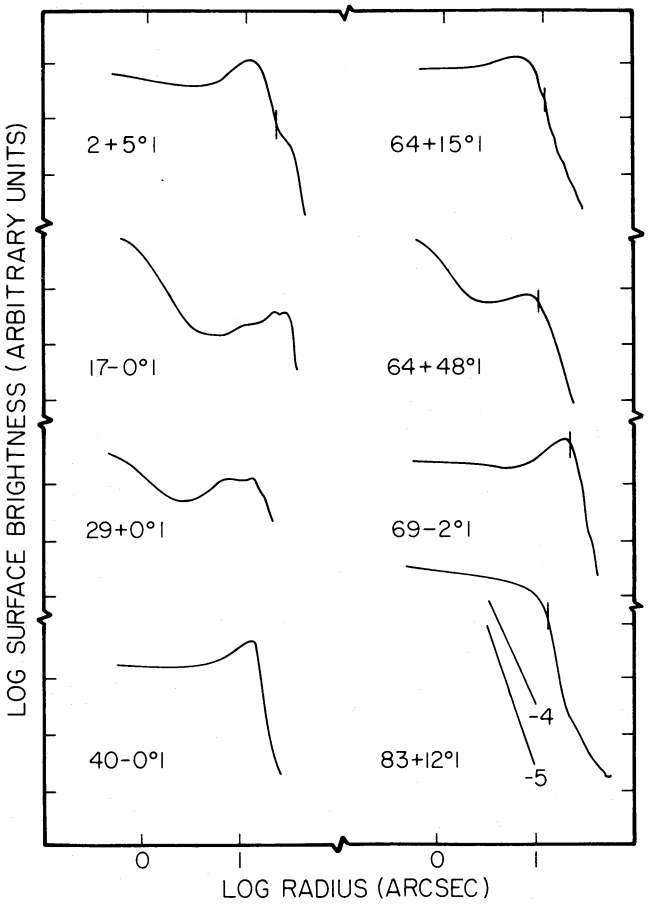

FIG. 5.—Azimuthally averaged Hα + [N II] surface brightness plots of circularly symmetric nebulae. The logarithm of the surface brightness is plotted against the logarithm of the radial distance from the central star in arcsec. Vertical ticks mark the boundaries between primary and halo material in those nebulae which possess halos. Lines of slope −4 and −5 are shown for reference.

TABLE 3

ELECTRON DENSITY MEASUREMENTS

Object (1)	$\Delta\alpha$ (″) (2)	$\Delta\delta$ (″) (3)	L (″) (4)	r/R_p (5)	Type (6)	[S II] (λ6716/λ6731) (7)	log N_e (m^{-3}) (8)
2+5°1.....	11W	0N	11	0.65	P	0.59 ± 0.06	$9.59^{+0.15}_{-0.11}$
	14E	0N	11	0.82	P	0.70 ± 0.07	$9.39^{+0.13}_{-0.14}$
	28W	0N	6	1.65	H	0.80 ± 0.20	$9.19^{+0.38}_{-0.35}$
	32E	0N	10	1.88	H	1.00 ± 0.10	$8.85^{+0.16}_{-0.15}$
10+18°2.....	0E	2N	5	0.15	P	0.51 ± 0.05	$9.81^{+0.24}_{-0.15}$
	7W	2N	9	0.56	P	0.64 ± 0.06	$9.50^{+0.11}_{-0.11}$
35−0°1.....	10W	0N	8	0.71	P	0.89 ± 0.09	$9.02^{+0.18}_{-0.14}$
	13E	0N	16	0.93	P	0.86 ± 0.09	$9.08^{+0.17}_{-0.16}$
	25W	0N	22	1.79	H	1.14 ± 0.11	$8.63^{+0.17}_{-0.28}$
50+3°1.....	0E	12S	46	0.90	P	0.76 ± 0.08	$9.27^{+0.16}_{-0.15}$
68−0°1.....	12E	0N	8	1.50	H	1.10 ± 0.11	$8.70^{+0.16}_{-0.23}$
	12E	12S	8	2.12	P	1.00 ± 0.10	$8.85^{+0.16}_{-0.15}$
68+1°2.....	0E	0N	12	0.00	P	0.96 ± 0.10	$8.91^{+0.17}_{-0.15}$
	10W	0N	8	0.91	P	0.94 ± 0.09	$8.94^{+0.16}_{-0.14}$
	13E	0N	8	1.18	P	0.98 ± 0.10	$8.88^{+0.16}_{-0.15}$
89+0°1.....	0E	0N	15	0.00	P	0.63 ± 0.06	$9.52^{+0.12}_{-0.11}$
	0E	12S	27		H	0.79 ± 0.08	$9.22^{+0.15}_{-0.16}$
97+3°1.....	17E	0N	29	0.61	P	1.29 ± 0.13	$8.22^{+0.37}_{-0.42}$
102−2°1.....	22E	0N	23	0.88	P	1.16 ± 0.12	$8.59^{+0.20}_{-0.34}$
	29W	0N	24	1.16	P	1.20 ± 0.12	$8.49^{+0.24}_{-0.38}$
	48E	0N	10	1.92	P	1.25 ± 0.13	$8.35^{+0.31}_{-0.43}$
103+0°1.....	27W	6S	31	1.73	P	0.94 ± 0.09	$8.94^{+0.16}_{-0.14}$
107+2°1.....	6W	0N	8	0.60	P	0.68 ± 0.07	$9.43^{+0.12}_{-0.14}$
	11E	0N	13	1.10	P	0.58 ± 0.06	$9.61^{+0.16}_{-0.11}$

statistical error distribution within the effective slit and are generally due to photon noise; column (8), log (N_e) m^{-3}: the logarithm of the electron density within the effective slit, and its formal uncertainty. The electron density was estimated from the [S II] (6717/6731) line ratio using the collision strengths calculated by Pradhan (1976) and the transition probabilities of Wiese, Smith, and Glennon (1966). An electron temperature $T_e = 10^4$ K was assumed.

An additional five nebulae had surface brightnesses high enough to permit the determination of spatially resolved electron densities. Results from these nebulae are not given in Table 3 but instead are plotted in Figures 6*a–e*. From these plots the general trend toward smaller electron densities in the halos may be followed. The rate of decrease is relatively slow. By inspection, the plots seem to preclude variations of the form $N_e(r) \propto r^{-n}$ with $n > 2$. However, the plotted measurements of the electron densities in the halos most likely represent only upper limits to the true spatially averaged halo electron densities. This is because regions of locally enhanced density will tend to have higher surface brightness than surrounding regions and will therefore be preferentially conspicuous in the slit spectra. The bright filamentary structures present in many halos (e.g., see 2+5°1, 25−4°2, 83+12°1) probably represent regions of locally enhanced density. A rough estimate of the magnitude of the density enhancement may be obtained by comparing the surface brightness of the filaments to the surface brightness of adjacent halo material. The surface brightness in a recombination line (e.g., Hα 6563 Å) varies as

$$B_r \propto N_e N_i \alpha(T_e) L ,$$

where N_e and N_i are the electron and ion densities, $\alpha(T_e)$ is the recombination coefficient appropriate for the line of interest, and L is the line-of-sight path length through the emitting region. Denoting filamentary properties "fil" and adjacent halo properties "h" we may take $B_{\rm fil}/B_h \approx 5$ and $L_{\rm fil}/L_h \approx 0.1$ from observations. Provided the filament and general halo electron temperatures are similar, we may take $\alpha_{\rm fil}/\alpha_h \approx 1$, since α is a very weak function of temperature. Furthermore, in a pure hydrogen nebula $N_e = N_i$, giving $N_e({\rm fil})/N_e(h) \approx 7$. This suggests that the measured electron densities, which are biased toward the densities in the filaments, overestimate the locally averaged electron densities by about a factor of 7. This is comparable to the filament density enhancement estimated by Capriotti (1973) from dynamical considerations. Considerably larger density enhancements have been proposed by Wentzel (1976).

The mean electron density in five planetary nebula halos, corrected as above for observational bias, is $N_e = 1.4 \times 10^8$ m^{-3} (140 cm^{-3}). This is equal to about 1/10th the typical electron density in the primary nebulae (Table 3). Taking $R_h/R_p = 2$ (§ III*a*) gives the ratio of the halo volume to the primary nebula volume to be ~10. Hence, by this argument, the order of magnitude of the ratio of the halo mass to the primary nebula mass is $M_h/M_p \approx 1$.

IV. INTERPRETATION

We consider four independent models of the origin of the nebular halos. The models, and others derived from them, have been previously proposed by other workers to account for the existence of individual halo nebulae. While each model may successfully represent some of the nebulae studied in this

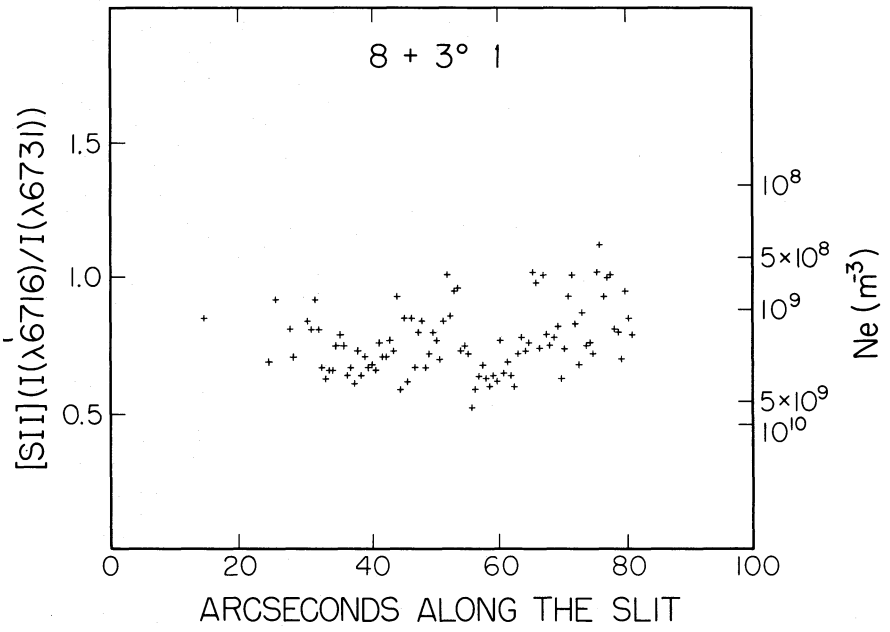

FIG. 6a

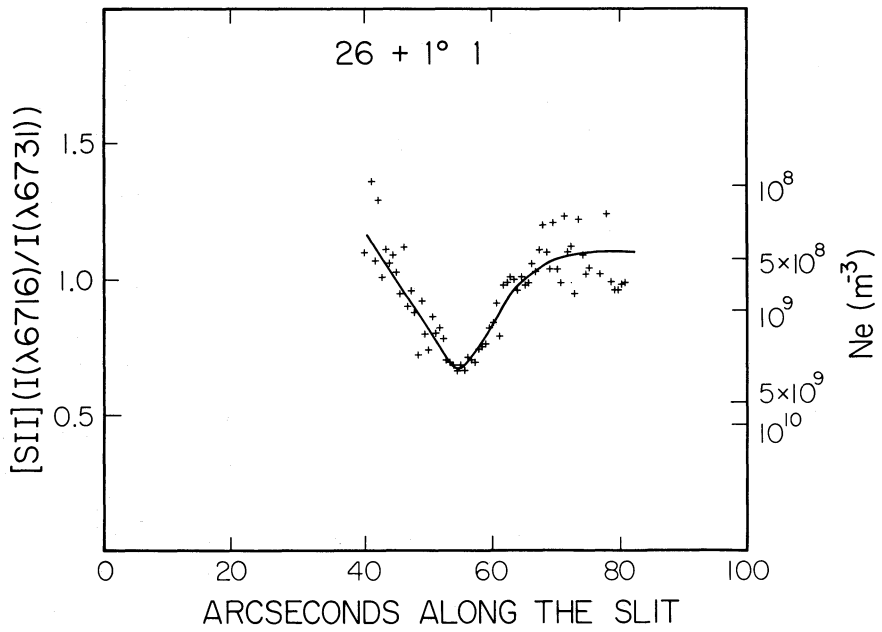

FIG. 6b

FIG. 6.—Variation of [S II] 6716, 6731 Å line intensity ratio and of electron density, log [N_e (m^{-3})], as a function of distance along slits projected east-west on the surfaces of five nebulae. The points represent measurements along single lines of pixels parallel to the dispersion. The statistical uncertainties in the line ratio at each slit position are indicated by the local scatter of the measurements. Very uncertain measurements have been omitted for clarity. The continuous lines, where drawn, have been added to guide the eye.

survey, our objective is to determine the model which is best able to represent a majority of the nebulae.

The halos might be caused by the scattering of nebular radiation from interstellar dust grains, as occurs in normal reflection nebulae. This model has been proposed by Atherton *et al.* (1979) to account for the halo surrounding NGC 7027. Several observations are inconsistent with this model of planetary nebula halos. (a) The optical spectra of the halos are generally different from the spectra of the respective primary nebulae. However, scattering of the radiation by dust grains would be nearly gray and could not produce the variations of emission line ratios as are observed. (b) Polarization measurements of the halos of 63+13°1 and 64+48°1 show that the linear polarization is $POL < 0.05$ at the wavelength of Hα. Typical reflection nebulae are observed to exhibit larger polarizations in the range $0.05 < POL < 0.15$ (Zellner 1973). (c) The large frequency of occurrence of halo nebulae reported in the present study would imply an unreasonably high coincidence between the spatial location of planetary nebulae and of interstellar dust clouds. Furthermore, high galactic latitude planetaries

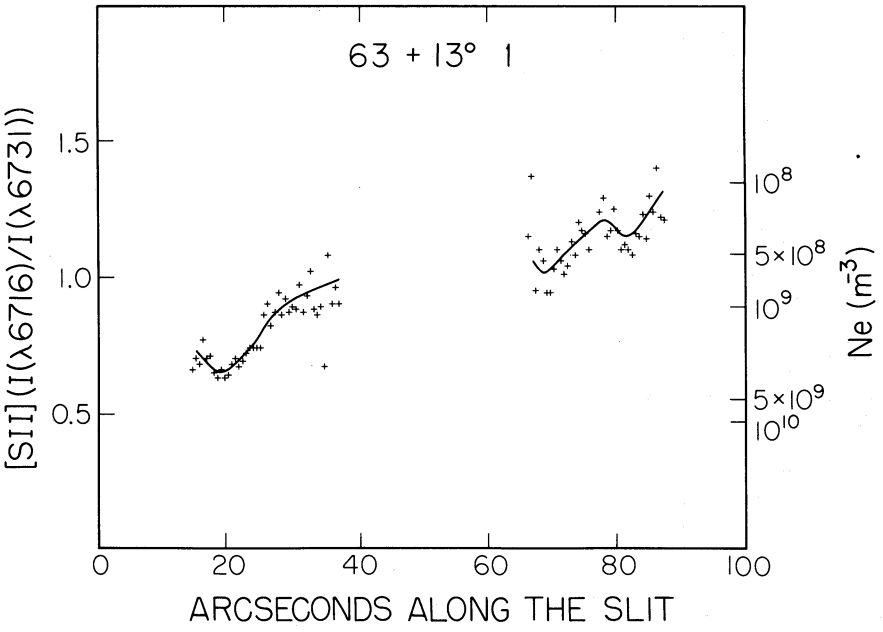

FIG. 6*c*

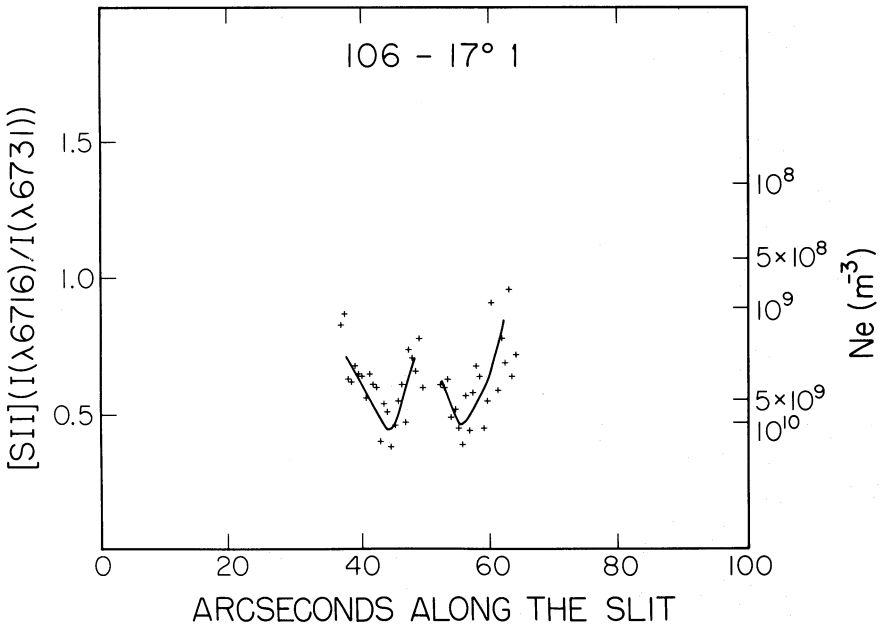

FIG. 6*d*

such as 64+48°1 ($b^{II} = +48°1$) and 96+29°1 ($b^{II} = +30$) possess conspicuous halos even though the interstellar medium at such large b^{II} is, presumably, very rarified. (d) The planetary nebula halos commonly exhibit a characteristic filamentary morphology which is not similar to the morphology of a typical reflection nebula. In view of the above mentioned arguments, it seems very unlikely that a majority of the halos might be due to reflection nebulae.

The halos might be due to excitation of the escaping stellar wind formerly produced by the central star when in a cool preplanetary red giant state (see, e.g., Kwok, Purton, and Fitzgerald 1978; Kwok 1982). Typical stellar wind mass-loss rates from red giant stars are observed to lie in the range $10^{-8} < dM/dt(M_\odot\ \mathrm{yr}^{-1}) < 10^{-6}$ (Cassinelli 1979). Exceptional stars, including the long-period variables often cited as progenitors of planetary nebulae, have $dM/dt \leq 10^{-5}\ M_\odot\ \mathrm{yr}^{-1}$. Such a wind expanding isotropically at the stellar escape speed from a star of mass $\approx 1\ M_\odot$ and radius $\approx 1000\ R_\odot$ would have a number density $N_w(\mathrm{m}^{-3}) \leq 10^{39} R^{-2}$, at distance $R(m)$ from the central star. The observed planetary nebula halos extend to at least $R \approx 0.5$ pc $\approx 1.5 \times 10^{16}$ m (Table 2). At this distance the stellar wind would have a number density $N_w < 4 \times 10^6$ m^{-3}. N_w may be compared with the halo electron densities listed in Table 3. There it is seen that typical halo filament electron densities are $N_e(h) \approx 1 \times 10^9\ \mathrm{m}^{-3}$. Allowing for an estimated factor of 7 density enhancement in the halo filaments

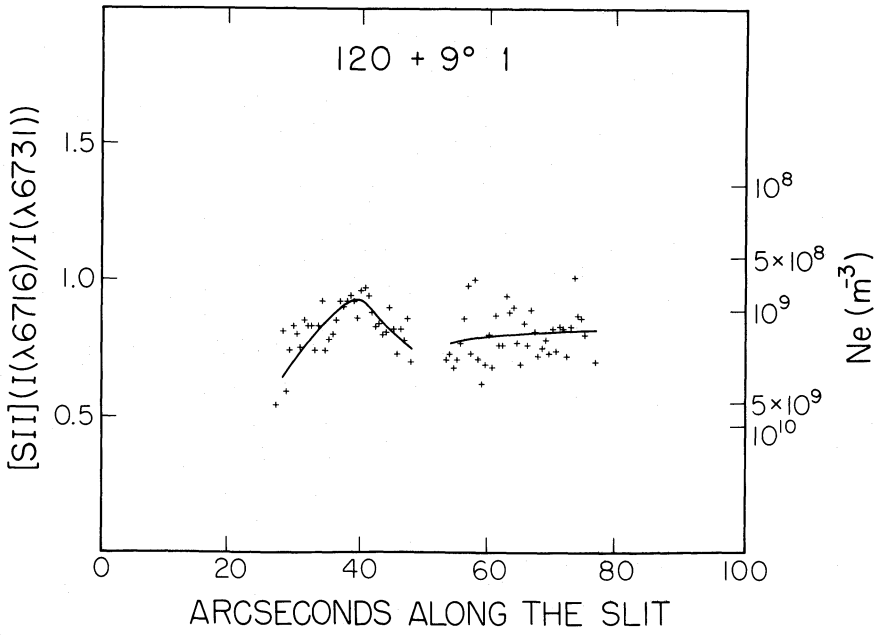

FIG. 6e

(§ IIIc) gives $N_e(h) \approx 1 \times 10^8$ m^{-3} which is still more than an order of magnitude larger than N_w. Hence, it is apparently unlikely that the planetary nebula halos are caused by excitation of escaping stellar winds unless the winds are stronger than we have assumed here. However, the uncertainties are large enough that we cannot discount the possibility that at least some of the halos may be due to such a process. Mass-loss rates exceeding 10^{-4} $M_\odot$ yr^{-1}, if sustained for the nebular expansion time $\sim 10^4$ year, would be able to produce the observed halo densities. Interestingly, Knapp *et al.* (1982) report mass loss rates approaching 10^{-4} $M_\odot$ yr^{-1} in some stars.

Excitation of the interstellar medium is unlikely to give rise to observable emission since the number densities there are very small, generally $< 10^6$ m^{-3}.

The halos might represent excited gas which is expanding away from but which originated in the primary nebula shell. The halo would be formed by dynamical separation from the primary shell after its ejection from the central star. Models of this type have been computed by Mathews (1966). The outer layers of the shell undergo accelerated expansion down the pressure gradient into the relative vacuum of interstellar space. Simple considerations lead to a model of the nebula in which the radial expansion speed, v, is proportional to the distance from the central star, R. The halo consists of gas which has accelerated away from the primary nebula. Taking $v \propto R$, the condition of continuity gives $N(R) \propto R^{-3}$, where N is the total number density of particles at R, and the expansion is assumed to be spherically symmetric. Assuming N_e/N = constant (i.e., tantamount to the assumption that the hydrogen Strömgren sphere is larger than the radius of the halo), and assuming constant electron temperature, the halo surface brightness in a recombination line (e.g., Hα) would vary as $B \propto R^{-5}$. Detailed calculations by Mathews in which the previous two assumptions are relaxed yield similarly steep surface brightness variations. Comparison with the halo surface brightness profiles shown in Figure 5 suggests that accelerated expansion models of this type may be able to reproduce the planetary nebula halos. However, the model profiles are sensitive to the net heating rate in the expanding gas and the heating rate is very poorly constrained by existing observations. In the absence of more rigid constraints, in the form of resolved electron density and temperature maps of specific halos, it would seem to be premature to perform model fitting. Hence, we conclude that this model may be consistent with the halo observations, but that a firm conclusion cannot yet be reached.

The planetary nebula ejection mechanism may lead to the production of two or more separate expanding shells, ejected from the central star at different times. We can find no strong observational test of this model in our data. However, one relevant observation is that the halo material usually appears contiguous with the primary nebula. There is rarely a case in which the supposed halo ejection occurred so long before the primary nebula ejection that a prominent gap exists between the halo and primary shells. Unless there is some fundamental limit to the length of time between successive ejections from the central star, this observation would seem to provide an argument against the multiple ejection model.

Further discrimination between the above formation mechanisms might be possible using radial velocity measurements of the halos. For instance, in the red giant wind model of Kwok we would expect to find a ratio of halo velocity to primary nebula velocity $v_h/v_p < 1$, since typical stellar wind speeds are only a fraction of the typical planetary nebula expansion speeds. Conversely, the accelerated expansion models of Mathews predict $v_h/v_p > 1$.

V. SUMMARY

1. Twenty-nine out of 44 randomly selected nebulae for which deep CCD images were taken are found to possess halos.

2. The halos exhibit a wide range of properties. The relative radii are concentrated in the range $1.1 < (R_h/R_p) < 5$, with an average $R_h/R_p \approx 2$. Many halos exhibit filamentary structure.

3. The apparent long axes of the primary nebulae are distributed randomly in direction. There is no evidence for the

axis alignment reported by Grinin and Zvereva (1967) and by Melnick and Harwit (1975).

4. The spatially averaged electron densities in five halos average $N_e \approx 10^8$ m^{-3}, about 10% of the densities of the primary nebula shells. Filaments in the halos have about 7 times the mean electron density. The ratio of the halo mass to the main shell mass is of order 1.

5. The halos are unlikely to be produced by scattering from interstellar dust nebulae. Some halos may be produced by excitation of preplanetary winds. It is likely that most halos result from either the dynamical separation of a single ejected shell or from the multiple ejection of shells from the central star. In future work, expansion velocity measurements will be used to discriminate between these models.

We thank J. A. Westphal and J. E. Gunn for permission to use the PFUEI. We are thankful for the skilled operation of the telescopes by Juan Carrasco, Al Lilge, Skip Staples, and Dave Tennant. Mike Ravine, Sid von Grollik, and Barbara Zimmerman provided valuable assistance during some of the observing runs.

REFERENCES

Acker, A. 1979, *Astr. Ap. Suppl.*, **33**, 367.
Atherton, P. D., Hicks, T. R., Reay, N. K., Robinson, G. J., Worswick, S. P., and Phillips, J. P. 1979, *Ap. J.*, **232**, 786.
Capriotti, E. R. 1973, *Ap. J.*, **179**, 495.
Cassinelli, E. R. 1979, *Ann. Rev. Astr. Ap.*, **17**, 275.
Curtis, H. D. 1918, *Pub. Lick. Obs.*, **13**, 57.
Duncan, J. C. 1937, *Ap. J.*, **86**, 496.
Greig, W. E. 1971, *Astr. Ap.*, **10**, 161.
Grinin, V. P., and Zvereva, A. M. 1968, in *IAU Symposium 34, Planetary Nebulae*, ed. D. E. Osterbrock and C. R. O'Dell (Dordrecht: Reidel).
Gunn, J. E., and Westphal, J. A. 1981, *Proc. S.P.I.E.*, **290**, 16.
Hamilton, N., and Liller, W. 1972, *Mem. Soc. Roy. Sci. Liége*, 6th Ser., **5**, 213.
Hunter, J. H., and Sofia, S. 1971, *M.N.R.A.S.*, **154**, 393.
Kaler, J. B. 1974, *A.J.*, **79**, 594.
Khromov, G. S., and Kohoutek, L. 1968, *Bull. Astr. Soc. Czechoslovakia*, **19**, 1.
Knapp, G. R., Phillips, T., Leighton, R. B., Lo, K. Y., Wannier, P. G., Wootten, H. A., and Huggins, P. J. 1982, *Ap. J.*, **252**, 616.
Kwok, S. 1982, *Ap. J.*, **258**, 280.
Kwok, S., Purton, C. R., and Fitzgerald, P. M. 1978, *Ap. J. (Letters)*, **219**, L125.
Mathews, W. G. 1966, *Ap. J.*, **143**, 173.
Melnick, G., and Harwit, M. 1975, *M.N.R.A.S.*, **171**, 441.
Millikan, A. G. 1974, *A.J.*, **79**, 11.
Minkowski, R., and Osterbrock, D. E. 1960, *Ap. J.*, **131**, 537.
Osterbrock, D. E., Millier, J. S., and Weedman, D. W. 1966, *Ap. J.*, **145**, 697.
Perek, L., and Kohoutek, L. 1967, *Catalogue of Galactic Planetary Nebulae, Prague.*
Pradhan, A. K. 1978, *M.N.R.A.S.*, **184**, 89P.
Reimers, D. 1977, *IAU Colloquium 42, The Interaction of Variable Stars with Their Environment*, ed. R. Kippenhahn, J. Rahe, and W. Strohmeier (Bamberg: Remeis-Sternwarte).
Weedman, D. W. 1968, *Ap. J.*, **153**, 49.
Wentzel, D. G. 1976, *Ap. J.*, **204**, 452.
Wiese, W. L., Smith, M. W., and Glennon, B. M. 1966, *Atomic Transition Probabilities: A Critical Data Compilation* (Washington, D.C.: U.S. National Bureau of Standards, Government Printing Office).
Wilson, O. C. 1950, *Ap. J.*, **111**, 279.
Zellner, B. 1973, in *IAU Symposium 52, Interstellar Dust and Related Topics*, ed. J. M. Greenberg and H. C. Van De Hulst (Dordrecht: Reidel), p. 109.

G. E. DANIELSON: 170-25, Caltech, Pasadena, CA 91125

DAVID C. JEWITT: 54-418 M.I.T., Cambridge, MA 02139

P. N. KUPFERMAN: 12-34, J.P.L., 4800 Oak Grove Drive, Pasadena, CA 91127

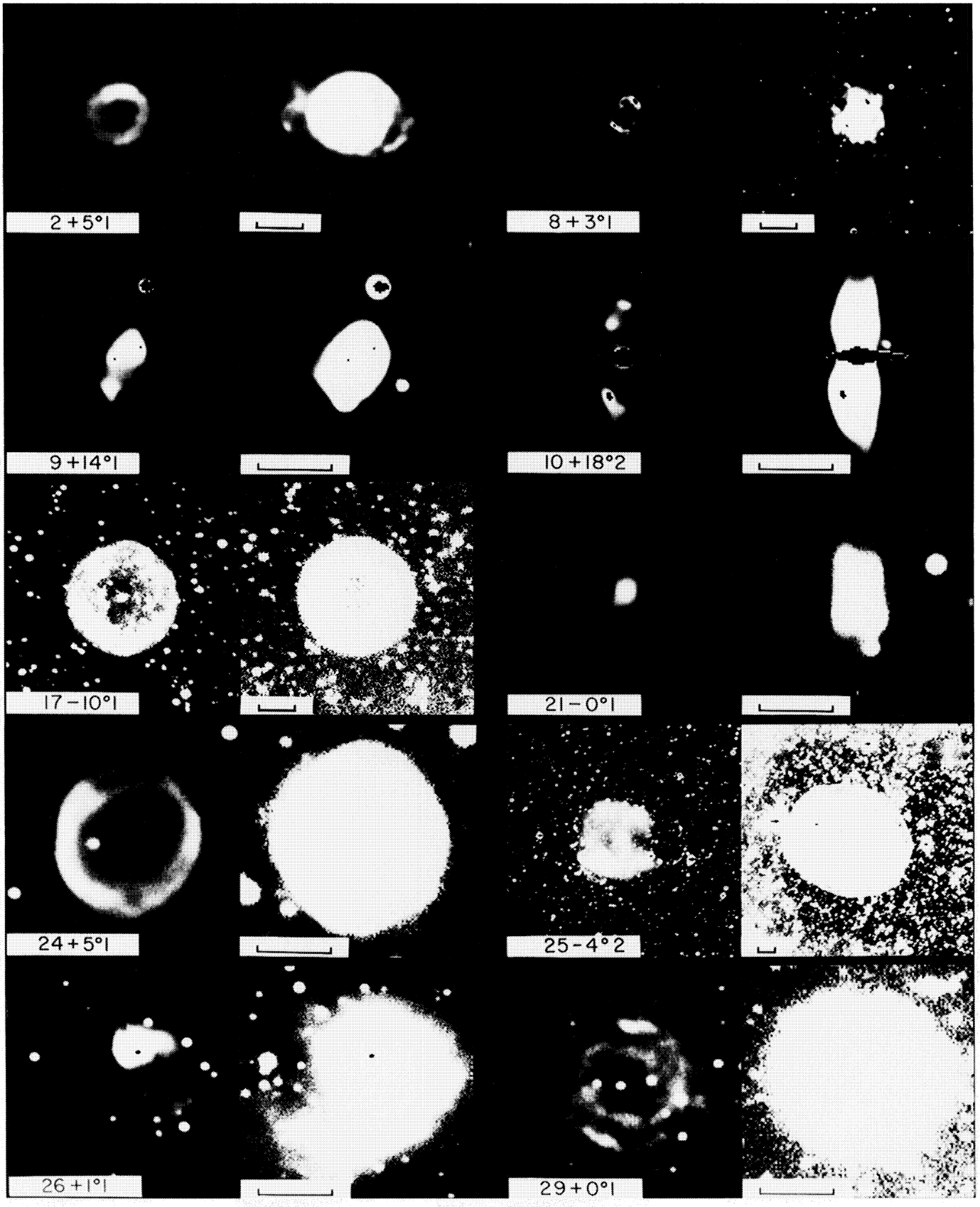

FIG. 1.—CCD images of planetary nebulae. Each nebula is shown twice. The left-hand image shows all data numbers between the sky brightness and the peak nebular brightness; the right-hand image shows the lowest 10% of the data numbers. The left-hand image emphasizes the primary nebula, whereas the right-hand image emphasizes the halo in nebulae where one is present. Saturated star images appear as black streaks. Each picture has north to the top, east to the left. The scale bars are each 20″ long.

PLATE 23

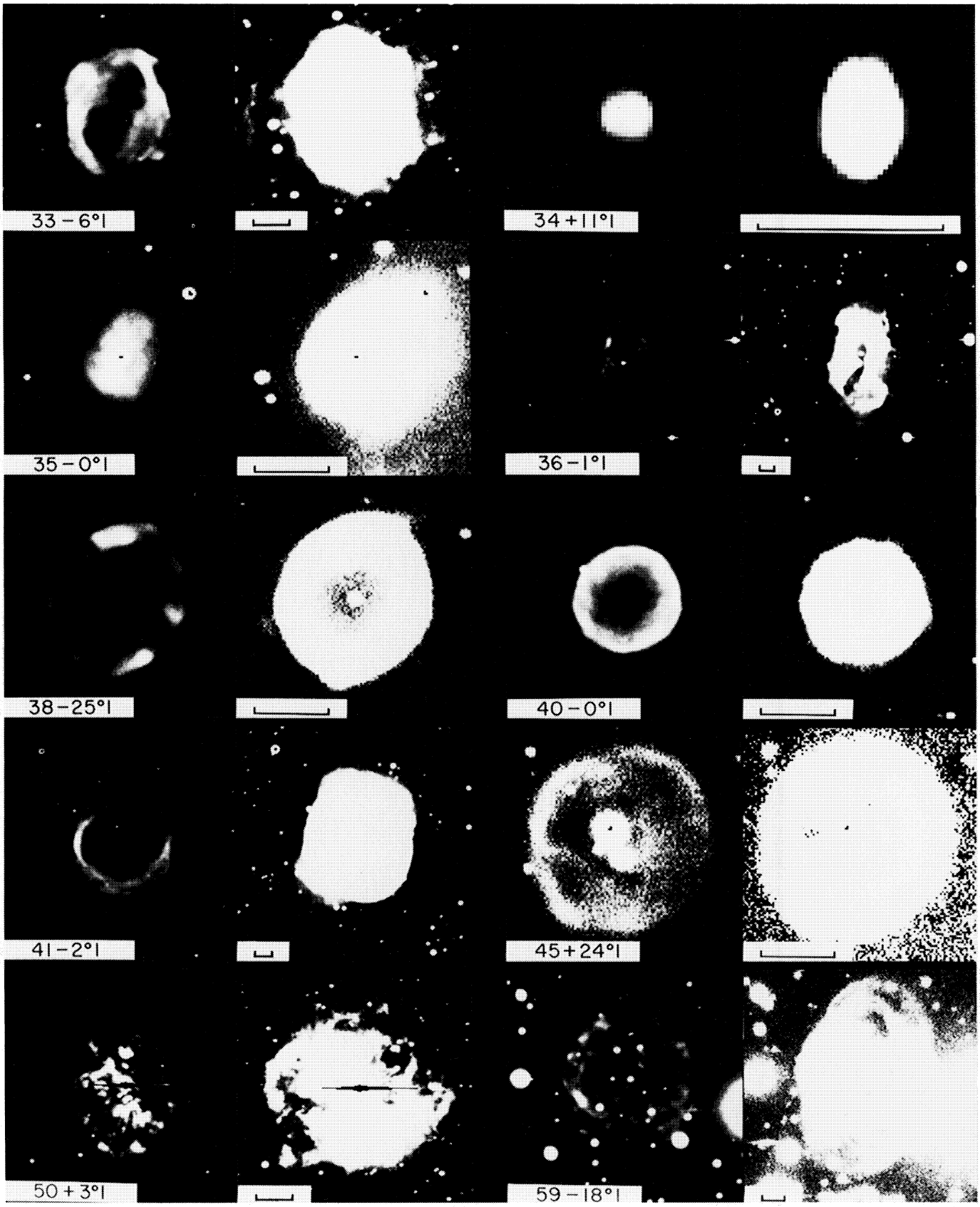

FIG. 1—*Continued*

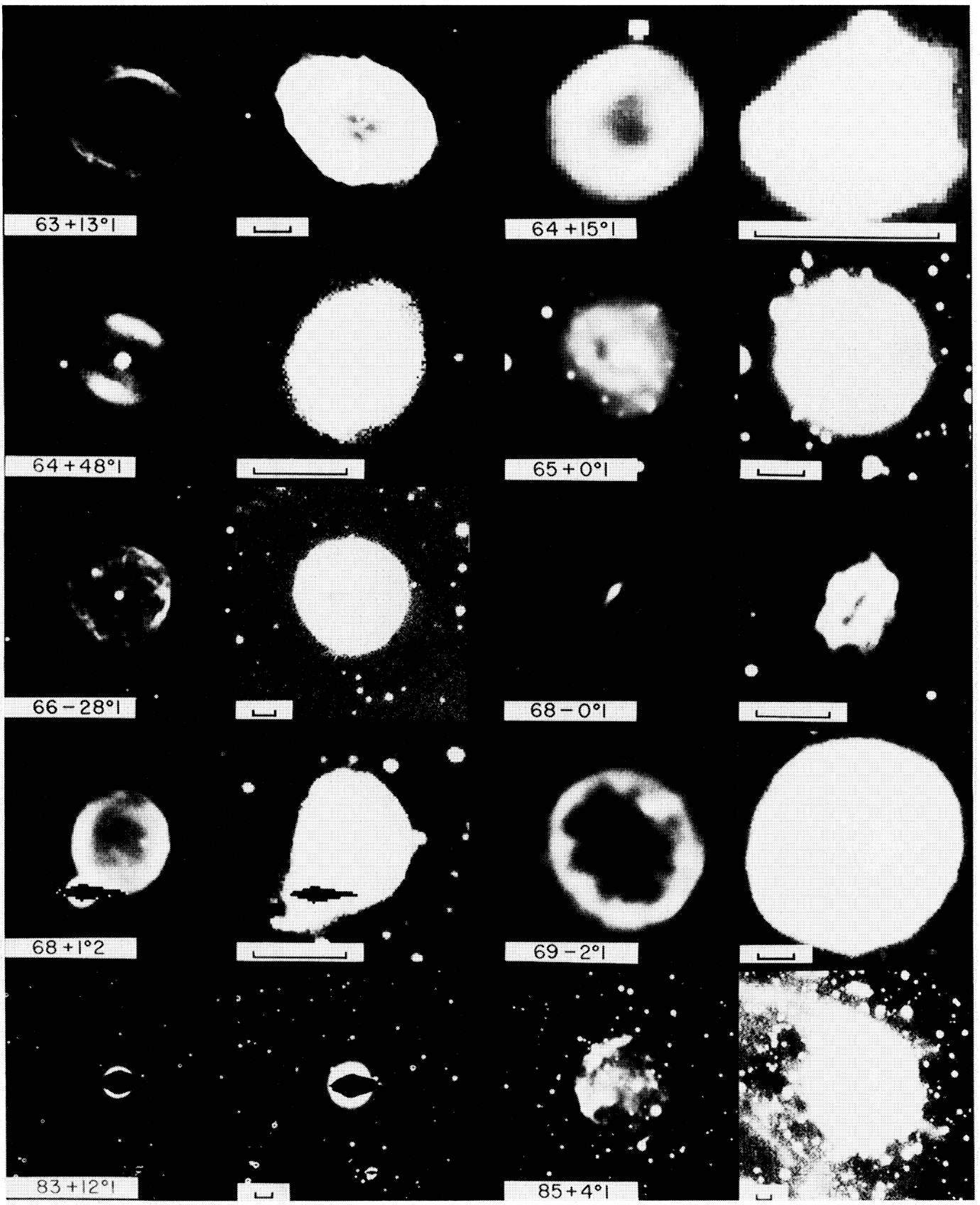

FIG. 1—*Continued*

JEWITT, DANIELSON, AND KUPFERMAN (*see* page 729)

PLATE 25

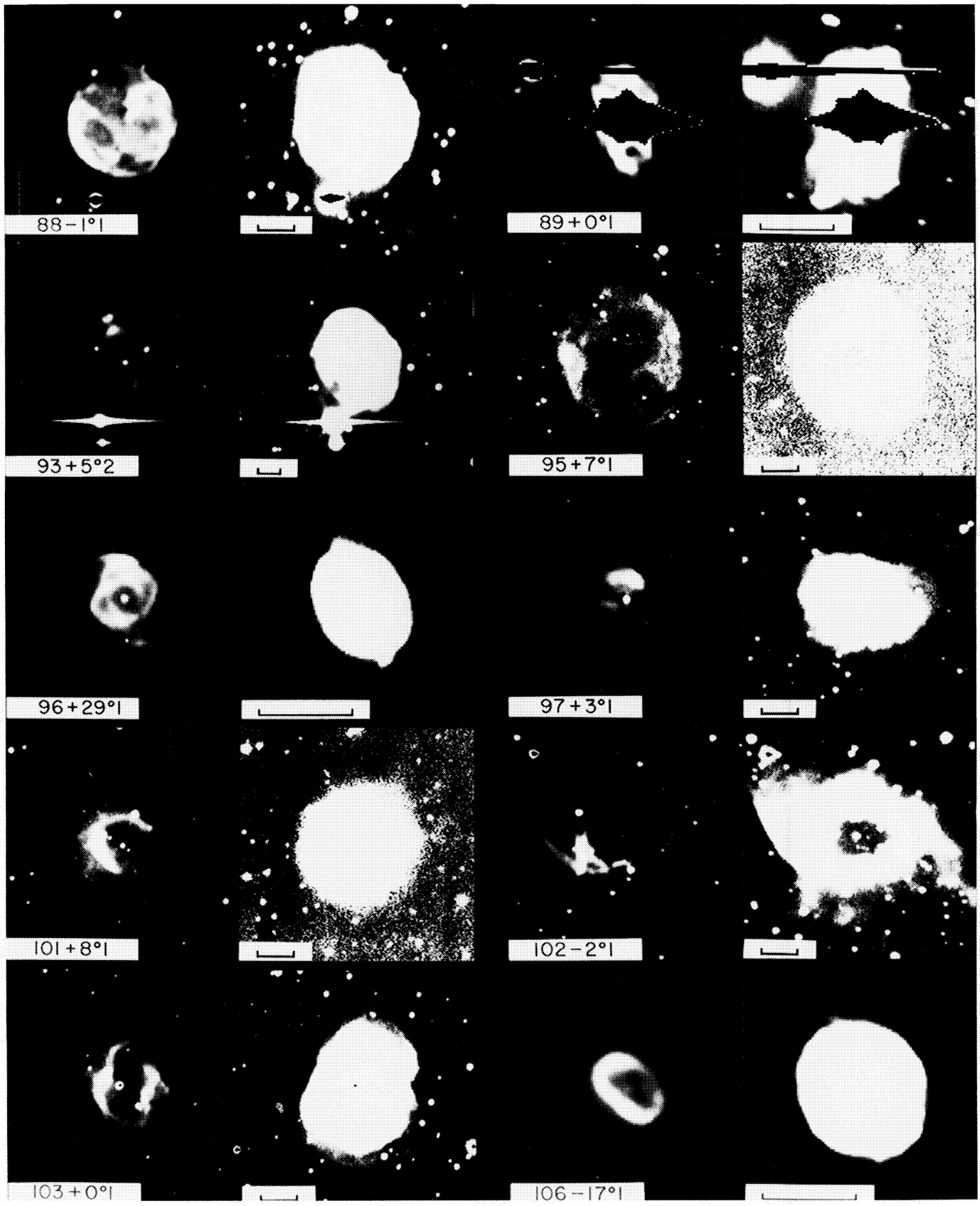

FIG. 1—*Continued*

JEWITT, DANIELSON, AND KUPFERMAN (*see* page 729)

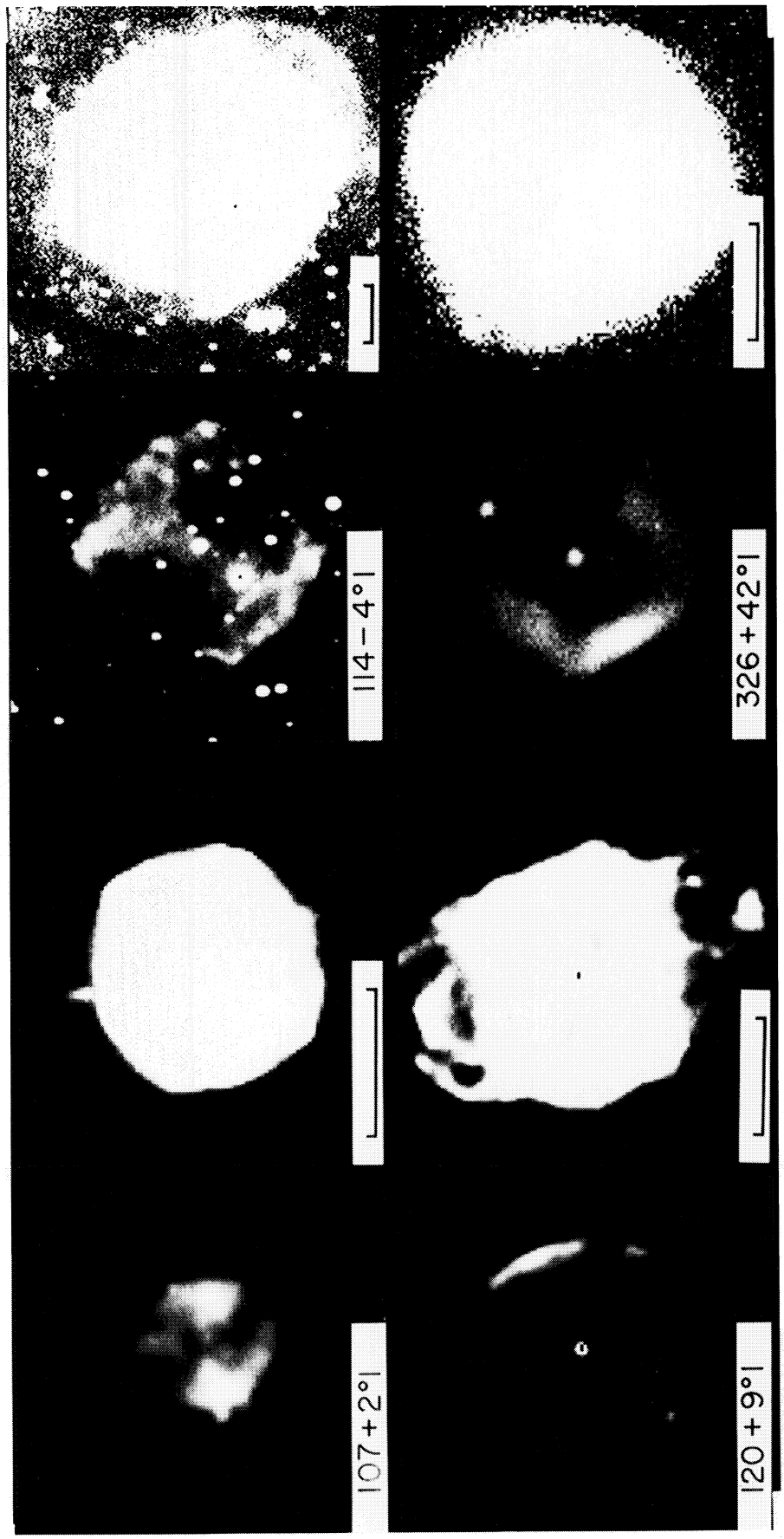

FIG. 1—*Continued*

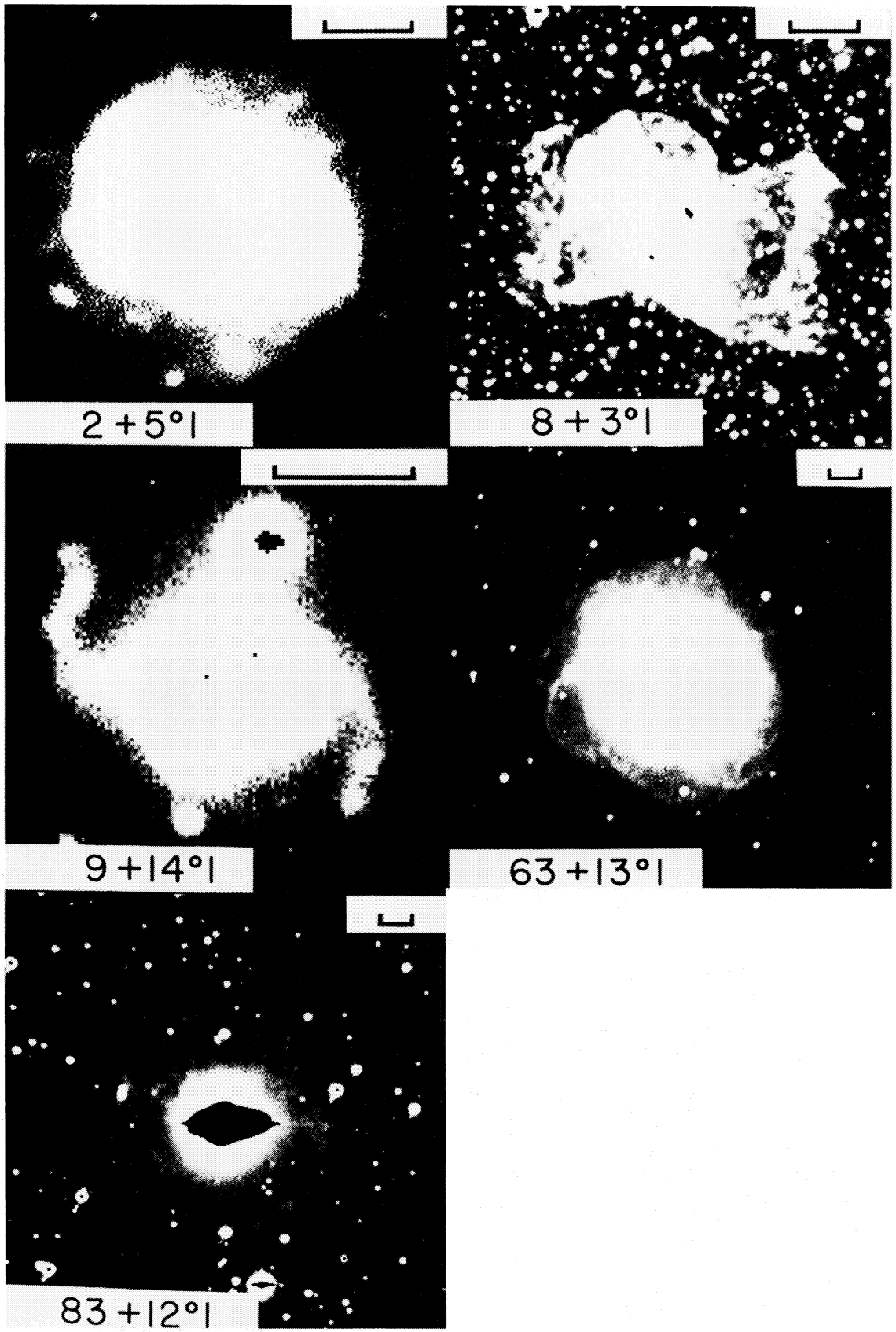

FIG. 2.—Stronger stretches of selected nebulae from Fig. 1. Only the lowest 1% of the data numbers are shown. The images emphasize very faint halos not well seen in Fig. 1. North is to the top, east to the left. The scale bars are each 20″ long.

JEWITT, DANIELSON, AND KUPFERMAN (*see* page 729)